Chemical Engineering Journal 105 (2005) 99–109

Chemical Engineering Journal

www.elsevier.com/locate/cej

Nonlinear phenomena and qualitative evaluation of risk of clogging in a capillary microreactor under imposed electric field

Michal Přibyl*, Dalimil Šnita, Miloš Marek

Department of Chemical Engineering and Center for Nonlinear Dynamics of Chemical and Biological Systems, Institute of Chemical Technology, Prague, Czech Republic

Received 13 July 2004; received in revised form 18 October 2004; accepted 23 October 2004

Abstract

Electric field imposed on a microchip, when electrokinetic pumping is used, can cause precipitation of electrolyte components and consequential clogging of the microchannels. We have found that the precipitation will occur in much broader range of electrolyte concentrations than in the case without the imposed electric field. For example, concentrations of the ions in the physiological fluids analyzed in the diagnostic microchips can also reach the solubility product when the gradient of the electric potential is used. This follows from the study of the mathematical model of the electrolyte transport and ionic interactions in microcapillaries.

The studied microsystem consists of two reservoirs containing aqueous electrolytes, a solution of potassium carbonate and a solution of calcium chloride, separated by a microcapillary containing a hydrogel. As the calcium and the carbonate ions diffuse and/or migrate in electric field in the microcapillary, calcium carbonate is formed and the risk of clogging increases at the locations where the concentration product of the calcium and carbonate ions exceeds the $CaCO_3$ solubility product.

Two qualitatively different spatio-temporal concentration patterns in the microcapillary of finite length in dependence on the applied difference of the electric potential have been found by means of the dynamical analysis. We have observed patterns with one and two maxima on the spatial profile of reaction rate of the calcium–carbonate interaction. Bifurcation diagram, in which the peak splitting has been clearly detected, was computed in dependence on the imposed gradient of electric potential. The peak splitting and thus the possibility of more complex precipitation patterns in the microcapillary follow from the existence of the sigmoidal profile of the electric potential arising in the presence of electric field. We have also found that the existence of sigmoidal profile strongly modifies the transport times of the chemical ionic components ($t_p \approx \Delta\Phi^{-1/3}$ in a broad range of applied gradient of electric potential $\Delta\Phi/l \in \langle 0.02, 20\rangle\ \mathrm{kV\,m^{-1}}$).

As the mathematical description of the model system is spatially one-dimensional, the obtained results are applicable especially in capillary microsystems with a large length/diameter ratio (e.g., separation microchannels or microchannels for isoelectrical focusing).

Keywords: Microreactor; Microcapillary; Mathematical modeling; Clogging; Peak splitting; Non-linear phenomena; Dynamic simulation; Electrophoresis

1. Introduction

A microcapillary system with initially separated ionic components that can form a solid precipitate is an important model system for studies of the clogging of micropores or microcapillaries used in microdevices. Electric field either arises naturally in the capillaries due to varying concentrations of ionic species or is imposed on the microcapillary when electroosmotic dosing of liquids is used. Effects of the electric field on the course of an interaction between precipitating ions are studied in this paper.

Spatially one-dimensional electrolyte systems with various chemical interactions on an infinitely large domain were often studied [1–5]. The initial separation of the reaction components is usually considered to be in a single point on the infinite domain. Sinder et al. [1,2] dealt with a system of two competing reactions. The authors derived the time characteristics of the reaction zone. They observed that the spatial profile of the reaction rate can have

* Corresponding author. Tel.: +420 2 2435 3168; fax: +420 2 3333 7335.
E-mail address: michal.pribyl@vscht.cz (M. Přibyl).

1385-8947/$ – see front matter © 2004 Elsevier B.V. All rights reserved.
doi:10.1016/j.cej.2004.10.003

two maxima. Sinder and Pelleg [3] also studied a reversible reaction–diffusion system with a non-diffusing product. The authors explained the observed splitting of the reaction zone as an effect of the immobile component. Taitelbaum et al. [4] and Yen et al. [5] theoretically and experimentally studied the competing reactions of Cr^{3+} ions with xylenol orange and the corresponding pH dependences of the distribution of the reaction product. Reaction front splitting and temporary nonmonotonic behavior of the global reaction rate was observed.

The interest in microtechnology and nanotechnology in the last decade has evoked an intensive research on the electrokinetic phenomena in microstructures particularly on the effects of the electric field on processes inside microcapillaries and more complex microstructures [6–9]. An external electric field can evoke electroosmotic flow inside the microreactor and thus the electroosmotic transport of electrolytes is widely used for dosing, pumping, and mixing in microchannels. Electroosmosis together with the electromigration can strongly affect the reaction rates in heterogeneous systems due to elimination of mass transfer resistance [10]. The authors looked for the regimes accelerating a bioaffinity reaction in the capillary microreactor. The employment of the Poisson equation enabled dynamical study of the processes near the phase interfaces within the microsystem.

In this work, we have chosen an electrolyte microsystem (see Fig. 1) with initially separated ionic components that can form a solid precipitate. A water solution of calcium chloride as one electrolyte and a water solution of potassium carbonate as the other one is the chosen example. The solid precipitate of calcium carbonate can be formed in the connecting microcapillary when the solubility product is exceeded. In the diagnostic microchips, samples of the physiological liquids can be analyzed. For example, physiological concentrations of calcium and bicarbonate ions in the blood plasma are usually about 2.5×10^{-3} and 2.5×10^{-2} kmol m^{-3} [11], respectively. Effects of similar concentrations of the ions and the intensity of an external electric field on the risk of microchannel clogging are studied in this work. Further, the formation of the solid calcium carbonate can play an important role in water treatment filters where the clogging of micropores can result in a substantial decrease of efficiency [12]. Precipitation of calcite is also observed in the water treatment

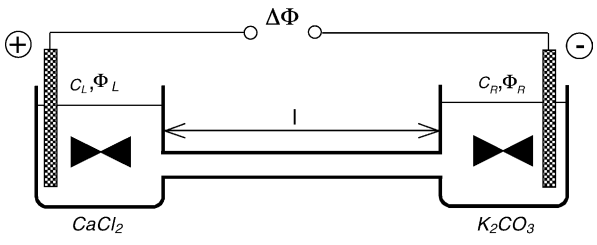

Fig. 1. Scheme of the reaction microsystem. The microcapillary connects two well-stirred reservoirs with constant values of concentrations and electric potential.

operations as a side product of the heavy metals precipitation by lime [13].

Many research groups use the formation of the solid phase from liquids in microchips to produce well-defined nano- and micro-particles. Chan et al. [14] exploited a microfluidic reactor for production CdSe nanocrystals. Takagi et al. [15] used a microcapillary device to produce TiO_2 particles. They avoided clogging by means of the two-phase flow when one liquid phase did not allow adhesion of the forming nanoparticles on the microcapillary walls. Wagner et al. [16] observed adsorption of the gold particles on the microchannels walls in the process of gold particle generation by citrate reduction. The operation parameters of the microdevice had to be precisely controlled in order to avoid the microchannel fouling. Schenk et al. [17] studied an organic synthesis accompanied by the precipitation of an ammonium salt in a microdevice. They found that small deviation in the volume flow in their chip can result in the microchannel clogging. Guillemet-Fritsch et al. [18] and Schenk et al. [19] use the segmented flow tubular microreactor for production of the nickel manganese oxalate powder and the calcite powder, respectively. This reactor contains large number of moving microreaction volumes in series separated by an immiscible fluid. Although this arrangement enables production of high quality powders, the risk of clogging is relatively high.

Extensive research has been focused on the modeling and experimental studies of clogging but the reports on the effects of an electric field on clogging are rare. Magnico [20] theoretically studied the evolution of clogging in a one-dimensional system by the deposition of a single chemical species. He analyzed qualitatively the coupling between the fluid transport, pressure gradients and chemical interactions. Hampton and Savage [21] investigated the evolution of clogging in a random pore network. Their results showed that permeability of the porous media depends on both the pore size distribution and the average pore size. Stole-Hansen [22] developed a dynamical model of the precipitation and dissolution processes in an electrolyte in a plug flow reactor. The precipitation processes can be used for the removal of impurities from an aqueous electrolyte. Stole-Hansen [22] considered the precipitation of $NiCO_3$, $Ni(OH)_3$, and PbO_2 and infinitely fast rate of the water and carbonic acid protolysis. He found that the precipitation in such type of reactor can be successfully controlled via pH level. Yu and Neretnieks [23] modeled transport and reaction processes including precipitation, electro-migration, and electroosmosis in a porous medium under the influence of an external electric field. They studied the removal of copper from sand by means of an external electric field in a case study. They found that the electrode reactions together with the reactions far away from the electrodes and the transport processes can form a steep pH jump somewhere in the porous medium. This jump constrains copper accumulation at this location. The insertion of a conductive solution next to the tube with sand resulted in a shift of the copper concentration maxima outwards. Hence, the external electric field can be used to remove some components

of the electrolyte out of the system and to avoid clogging of the system by a precipitate.

The chemical system with initially separated components leading to the precipitation can exhibit nonlinear behavior and form periodic spatial structures—Liesegang patterns [24]. The formation of periodic patterns of the solid precipitate is a result of several complex processes such as diffusion of the precipitating components, nucleation of the crystal centers, redissolution of the precipitate, kinetics of the particle growth, etc. The spatial distribution of the solid precipitate depends on the initial concentration of the reacting components, on distribution of the internal gradients of concentrations and temperature, on the presence of the gravitational field, etc. [25]. The effects of an external electric field on the structure of the Liesegang patterns and the speed of the front propagation were described in many papers, e.g. [26–29]. Sultan and Halabieh [26] and Lagzi [27] experimentally studied the propagating patterns of precipitation. They found that the dependence of the propagation velocity on the electric field strength can be nonlinear. An external electric field can also cause other nonlinear phenomena such as reaction wave splitting, stopping, symmetry breaking, etc., e.g. [30,31].

In our paper, we do not deal with the processes of precipitation occurring after the saturation limit has been reached (the nucleation or the crystal growth). We study the effects of an imposed electric field on the transport of ionic components, on the chemical interactions and on the attainability of the limit of solubility in the microreactor containing the aqueous electrolyte. We focus on the location of regimes that have a potential to establish the conditions that can lead to clogging of the microstructure. The microcapillaries with initially separated components in electric field are a typical arrangement used in the dosing via electroosmosis in microchips. We will demonstrate that the imposed electric field can substantially increase the risk of clogging and create complex concentration profiles of the precipitating ions.

2. Mathematical model

We consider the reaction microsystem depicted in Fig. 1. The system consists of two reservoirs and one connecting microcapillary. The L and the R reservoirs contain electrolytes of a particular composition: a solution of calcium chloride and a solution of potassium carbonate, respectively. These electrolytes are separated by a microcapillary containing a gel with no bound electric charge. As the calcium and the carbonate ions diffuse or migrate (under the influence of electric field) in the microcapillary, calcium carbonate is formed. The dissociation reactions of the carbonic acid, bicarbonate and water can also occur in the connecting microcapillary.

Let us consider that the reservoirs are well-stirred and the ionic composition of the reservoir solutions is approximately constant in time. A difference of electric potential can be imposed on the microsystem. Further, we assume that the electrode reactions and their products do not affect the processes inside the microcapillary system. These assumptions can be satisfied in typical microsystems.

The distribution of concentration of the ith component in the microcapillary connecting both reservoirs is described by the molar balance

$$\frac{\partial c_i}{\partial t} = -\nabla \cdot \vec{J}_i + \sum_{j=1}^{n} \upsilon_{ij} r_j, \quad i = 1, \ldots, m, \tag{1}$$

where the total flux of the ith component $\vec{J}_i$ is given by the sum of the diffusion and the electro-migration fluxes according to Nernst–Planck equation

$$\vec{J}_i = \vec{J}_i^D + \vec{J}_i^E = -D_i \nabla c_i - \frac{z_i D_i F}{RT} c_i \nabla \Phi. \tag{2}$$

Some components of the electrolyte can interact with other components in n chemical reactions (see Eq. (1)). The rate of formation of the ith component in the jth chemical reaction is given by the product of the stoichiometric coefficient and the expression for the reaction rate $\upsilon_{ij} r_j$. The symbol $\nabla\Phi$ in Nernst–Planck equation denotes the gradient of electric potential.

In our system, the longitudinal dimension l of the microsystem is dominant and the effects of the fixed electric charge on the internal microcapillary walls are neglected. The lateral dimensions of the microcapillary are usually of the order of several microns, whereas the considered range of the microcapillary length is $\langle 0.5, 50 \rangle$ mm. Hence we expect that a long-microcapillary system will be effectively spatially one-dimensional. After the application of the fin approximation [34] on the model equations, we receive the one-dimensional model that was analyzed in this study.

The distribution of electric potential is given by the solution of Poisson equation

$$\nabla \cdot (\nabla \Phi) = \frac{-q}{\varepsilon_r \varepsilon_0}, \tag{3}$$

where $\varepsilon_r \varepsilon_0$ denotes the permitivity of the solution. Here we consider a constant value of the permitivity in the entire system. The charge density q depends on the local composition of the electrolyte according to Eq. (4)

$$q = F \sum_{i=1}^{m} z_i c_i, \tag{4}$$

where z_i is the charge number of the ith component of the electrolyte, and F is the Faraday's constant.

Yu et al. [23] eliminated the Poisson equation from the mathematical description of precipitating reactions using the assumption of electroneutrality in the whole system. Lindner et al. [32] and Šnita et al. [33] proved that simple ionic systems can be far away from the electroneutrality under specific conditions (in the case of existence of phase–phase interfaces, fixed electric charge and/or steep concentration gradients). Hence we do not use the local electroneutrality assumption in the description of the system.

The composition of the reservoir solutions and the imposed electric potentials define the boundary conditions of the system. The Dirichlet boundary conditions with the constant vector of concentrations and constant value of electric potential are considered

$$c_i|_{x=0} = c_{i,\mathrm{L}}, \qquad c_i|_{x=\mathrm{L}} = c_{i,\mathrm{R}}, \qquad \Phi|_{x=0} = \Phi_{\mathrm{L}},$$
$$\Phi|_{x=\mathrm{L}} = \Phi_{\mathrm{R}}, \quad i = 1, \ldots, m. \tag{5}$$

In dynamical simulations, we consider a microcapillary filled with a hydrogel at pH = 7 as the initial condition of the microsystem.

Temperature changes arising from the released Joule heat and chemical reactions are usually negligible in such systems due to high ratio of internal surface and volume of the microcapillary. Therefore, the energy balance is not included in the mathematical model.

The interactions between the solutions of calcium chloride and potassium carbonate are the subject of this study. The calcium and the carbonate ions form calcium carbonate that can precipitate

$$\mathrm{Ca^{2+}} + \mathrm{CO_3{}^{2-}} \rightarrow \mathrm{CaCO_3}. \tag{6}$$

The solid precipitate of $CaCO_3$ can be stable if the value of the solubility product K_s is exceeded in the solution

$$K_s = c_{\mathrm{CO_3{}^{2-}}} c_{\mathrm{Ca^{2+}}}. \tag{7}$$

Let us assume that the reaction rate of $CaCO_3$ formation can be described by the second-order kinetic equation

$$r_1 = k_1 c_{\mathrm{CO_3{}^{2-}}} c_{\mathrm{Ca^{2+}}}. \tag{8}$$

Nancollas and Reddy [35] and Chong [36] studied the kinetics of calcium carbonate precipitation. They found that the rate of the crystal growth can be expressed by the second-order kinetics. In this paper, we have assumed that the formation of calcium carbonate (both the dissolved and the solid one) is controlled by the same kinetics. The rate of the backward dissociation of $CaCO_3$ is neglected. This assumption should be valid if the concentration of the dissolved $CaCO_3$ is low. Because the solubility of $CaCO_3$ is very low (given by the solubility product K_s), the above-mentioned assumption is usually satisfied. Here, we do not study the processes of precipitation and the crystal growth in the supersaturated electrolyte. We only want to detect such regimes in the parametric space where the formation of $CaCO_3$ is possible because the product of calcium and carbonate concentrations is higher than the value of the solubility product K_s. More general description of steady state distributions of concentrations and electric potential can also consider the backward dissociation of calcium carbonate, the dissolution of the solid form of $CaCO_3$, the $CaCO_3$ crystal formation and the changes of transport parameters of all components if the microcapillary clogging occurs. The steady state analysis of our simplified model can indicate possible supersaturation of the electrolyte in the microreactor and the existence of the possibility of crystal formation. Because we are looking for the regimes where the precipitation of $CaCO_3$ can cause microreactor clogging, we have to consider that any region of the microstructure, where the solubility product is exceeded, has a potential for the crystal formation. The kinetics expressed by Eq. (8) is thus suitable for dynamical analysis on the time interval between the introduction of the $CaCl_2$ and K_2CO_3 electrolytes into the contact and the time when the solubility product is exceeded for the first time. Hence the processes occurring in the supersaturated solution need not be considered for this type of computation because no solid $CaCO_3$ is present in the microreactor. The dynamical analysis can give us good indication of both the time and the position of the appearance of the first precipitate.

If K_2CO_3 is dissolved in water, carbonate exists in three forms depending on the pH value of the solution. Two dissociation/association interactions occur in such electrolytes

$$\mathrm{H_2CO_3} \overset{K_{\mathrm{a1}}}{\rightleftarrows} \mathrm{H^+} + \mathrm{HCO_3{}^-}, \tag{9}$$

$$\mathrm{HCO_3{}^-} \overset{K_{\mathrm{a2}}}{\rightleftarrows} \mathrm{H^+} + \mathrm{CO_3{}^{2-}}. \tag{10}$$

The reaction rates of these interactions are described by Eqs. (11) and (12)

$$r_2 = k_2(c_{\mathrm{H^+}} c_{\mathrm{HCO_3{}^-}} - K_{\mathrm{a1}} c_{\mathrm{H_2CO_3}}), \tag{11}$$

$$r_3 = k_3(c_{\mathrm{H^+}} c_{\mathrm{CO_3{}^{2-}}} - K_{\mathrm{a2}} c_{\mathrm{HCO_3{}^-}}). \tag{12}$$

Moreover, the recombination/dissociation reaction of water occurs

$$\mathrm{H^+} + \mathrm{OH^-} \overset{K_{\mathrm{w}}}{\rightleftarrows} \mathrm{H_2O}, \tag{13}$$

and the expression for its reaction rate can be written as

$$r_4 = k_4(c_{\mathrm{H^+}} c_{\mathrm{OH^-}} - K_{\mathrm{w}}). \tag{14}$$

The values of the equilibrium and the kinetic constants used in our simulation are summarized in Table 1.

The fast dissociation processes (9), (10), and (13) in the microsystem are often considered to be in equilibrium. However, the presence of a sharp gradient of the electric potential can lead to a deviation from the equilibrium because the electro-migration transport processes can be faster in such systems. As we are not definitely able to exclude the formation of such gradients in the microsystem, finite rates of the fast dissociation interactions are considered.

The electrolyte solutions in the reservoirs are considered to be in the reaction equilibrium and satisfy the condition of local electroneutrality. The following values of concentrations are chosen in the L reservoir: $c_{\mathrm{Cl^-,L}} = 2 \times 10^{-3}\,\mathrm{kmol\,m^{-3}}$, $c_{\mathrm{K^+,L}} = c_{\mathrm{H_2CO_3,L}} = c_{\mathrm{HCO_3{}^-,L}} = c_{\mathrm{CO_3{}^{2-},L}} = 0\,\mathrm{kmol\,m^{-3}}$, $\mathrm{pH_L} = 8.5$. The concentrations of hydroxyl and calcium ions are computed from the definitions of the water ionic product and local electroneutrality

$$K_{\mathrm{w}} = c_{\mathrm{H^+}} c_{\mathrm{OH^-}}, \tag{15}$$

Table 1
Model parameters

Parameter	Description	Value	Units
pH_L	pH value on the L boundary	8.5	1
$c_{Ca^{2+},L}$	Concentrations of calcium ions on the L boundary	1.0016×10^{-3}	kmol m^{-3}
$c_{Cl^-,L}$	Concentrations of chloride ions on the L boundary	2×10^{-3}	kmol m^{-3}
$c_{K^+,L}$	Concentrations of potassium ions on the L boundary	0	kmol m^{-3}
$c_{H_2CO_3,L}$	Concentrations of carbonic acid on the L boundary	0	kmol m^{-3}
$c_{HCO_3^-,L}$	Concentrations of bicarbonate ions on the L boundary	0	kmol m^{-3}
$c_{CO_3^{2-},L}$	Concentrations of carbonate ions on the L boundary	0	kmol m^{-3}
pH_R	pH value on the R boundary	8.5	1
$c_{Ca^{2+},R}$	Concentrations of calcium ions on the R boundary	0	kmol m^{-3}
$c_{Cl^-,R}$	Concentrations of chloride ions on the R boundary	0	kmol m^{-3}
$c_{K^+,R}$	Considered range of concentrations of potassium ions on the R boundary	1.323×10^{-5} to 10.08	kmol m^{-3}
$c_{H_2CO_3,R}$	Considered range of concentrations of carbonic acid on the R boundary	6.960×10^{-8} to 6.960×10^{-2}	kmol m^{-3}
$c_{HCO_3^-,R}$	Considered range of concentrations of bicarbonate ions on the R boundary	9.785×10^{-6} to 9.785	kmol m^{-3}
$c_{CO_3^{2-},R}$	Considered range of concentrations of carbonate ions on the R boundary	1.451×10^{-7} to 0.1451	kmol m^{-3}
D_{H^+}	Diffusion coefficient of protons	9.31×10^{-9}	m^2 s^{-1}
D_{OH^-}	Diffusion coefficient of hydroxyl ions	5.28×10^{-9}	m^2 s^{-1}
D_{Cl^-}	Diffusion coefficient of chloride ions	2.04×10^{-9}	m^2 s^{-1}
$D_{Ca^{2+}}$	Diffusion coefficient of calcium ions	7.0×10^{-10}	m^2 s^{-1}
D_{K^+}	Diffusion coefficient of potassium ions	1.96×10^{-9}	m^2 s^{-1}
$D_{H_2CO_3}$	Diffusion coefficient of carbonic acid	8.0×10^{-10}	m^2 s^{-1}
$D_{HCO_3^-}$	Diffusion coefficient of bicarbonate ions	8.0×10^{-10}	m^2 s^{-1}
$D_{CO_3^{2-}}$	Diffusion coefficient of carbonate ions	8.0×10^{-10}	m^2 s^{-1}
z_{H^+}	Charge number of protons	1	1
z_{OH^-}	Charge number of hydroxyl ions	−1	1
z_{Cl^-}	Charge number of chloride ions	−1	1
$z_{Ca^{2+}}$	Charge number of calcium ions	2	1
z_{K^+}	Charge number of potassium ions	1	1
$z_{H_2CO_3}$	Charge number of carbonic acid	0	1
$z_{HCO_3^-}$	Charge number of bicarbonate ions	−1	1
$z_{CO_3^{2-}}$	Charge number of carbonate ions	−2	1
F	Faraday constant	9.6487×10^7	C kmol^{-1}
R	Molar gas constant	8.314×10^3	J kmol^{-1} K^{-1}
T	Temperature	310	K
ε_0	Vacuum permittivity	8.8542×10^{-12}	F m^{-1}
ε_r	Relative permittivity of water	7.85×10^1	1
k_1	Kinetic constant of $CaCO_3$ formation	3.333	m^3 kmol^{-1} s^{-1}
k_2	Kinetic constant of carbonic acid formation	1.3×10^{10}	m^3 kmol^{-1} s^{-1}
k_3	Kinetic constant of bicarbonate formation	1.3×10^{10}	m^3 kmol^{-1} s^{-1}
	Kinetic constant of water recombination	1.3×10^{11}	m^3 kmol^{-1} s^{-1}
K_w	Ionic product of water	1×10^{-14}	kmol^2 m^{-6}
K_{a1}	Carbonic acid dissociation constant	4.446×10^{-7}	kmol m^{-3}
K_{a2}	Bicarbonate dissociation constant	4.688×10^{-11}	kmol m^{-3}
K_s	Solubility product of $CaCO_3$	8.7×10^{-9}	kmol^2 m^{-6}
v_x	Convective velocity	0	m s^{-1}

$$\sum_i z_i c_i = 0. \tag{16}$$

In the R reservoir, we choose $c_{Cl^-,R} = c_{Ca^{2+},R} = 0\,\text{kmol m}^{-3}$ and $pH_R = 8.5$. The total concentration of carbonate $c_{CO_3,R}$ is one of the investigated parameters and its value is specified in the figure captions. Concentrations of the other ions are computed by means of Eqs. (15)–(19)

$$K_{a1} = \frac{c_{H^+,R} c_{HCO_3^-,R}}{c_{H_2CO_3,R}}, \tag{17}$$

$$K_{a2} = \frac{c_{H^+,R} c_{CO_3^{2-},R}}{c_{HCO_3^-,R}}, \tag{18}$$

$$c_{CO_3,R} = c_{CO_3^{2-},R} + c_{HCO_3^-,R} + c_{H_2CO_3,R}. \tag{19}$$

3. Numerical analysis

The mathematical model consists of the molar balances (1), Poisson equation of electrostatics (3), and the initial and boundary conditions (5). The number of molar balances (1) describing the microcapillary system is $m = 8$: $i = H^+$, OH^-, Ca^{2+}, K^+, Cl^-, H_2CO_3, HCO_3^-, CO_3^{2-}. The model contains four interactions ($n = 4$ in Eq. (1)) with kinetics given by Eqs. (8), (11), (12) and (14). Analysis of steady state and dynamical analysis of the system with the interaction between precipitating ions is carried out in this

study. The developed numerical software is based on the Matlab/Femlab platform that uses the method of finite elements for the solution of partial differential equations (PDE). The requirements on the accuracy of solution demanded the use of spatial discretization of the model equations into 800 elements.

The time derivatives in Eq. (1) are equal to zero in the steady state analysis. The resulting set of ordinary differential equations of the second-order was solved. The extremely low value of the water permittivity and high values of the reaction rate constants induce stiffness of the solved equations. Hence we used imbedding approach, starting with such values of the parameters, for which we can get a solution of the model system. Further, we computed an error function depending on the gradients of concentrations and electric potential from the received solution. The distribution of the mesh elements was adapted according to the shape of the error function. Required values of the model parameters were used in the next round of computation. This procedure was repeated several times to receive the accurate steady state solution for the chosen model parameters.

An efficient algorithm had to be developed for the dynamical analysis. The set of parabolic PDEs (the molar balances) and one elliptic equation (Poisson equation) are solved numerically in this case. Sharp gradients in the concentration and potential profiles are observed particularly at the start of dynamical simulations. Further, these gradients move due to diffusion and migration of the electrolyte components. Hence the algorithm for dynamical simulations rebuilds the adaptive spatial mesh according to the chosen error function in specific time intervals that are estimated from the transport properties of ions. The distribution of the spatial mesh is also corrected in order to cover the migration length of ions with a dense mesh of elements in the next time interval. The implicit solver daspk [37] based on the backward differentiation formulae is used for time integration of the discretized set of model equations. A single dynamical simulation from the initial condition until the solubility limit is reached takes approximately 1 h on the PC 2.4 GHz.

4. Results and discussion

The external electric field is an important tool for the dosage and manipulation of the electrolyte solutions in microreactors. Hence our analysis is mostly focused on the effects of the imposed potential gradient and on the development of spatio-temporal patterns of ionic concentrations in the reservoirs. We assume that all phenomena studied in this paper occur far from the electrodes. Hence the local processes on the electrode surface do not affect the processes in the microcapillary. The gradients of the electric potential used in the simulations usually range from 0 to 100 V per 1 mm. It corresponds to values of electric field intensity in the interval from 0 to 100 kV m^{-1} that represents a typical situation in a microfluidic system (cf., e.g. [38]).

4.1. Steady state analysis

The analysis of steady states gives us only partial information about the effect of model parameters on the global behavior of the system because all dynamical and stability information are lost. However, the steady state analysis is a good indicator of the possibility of existence of local supersaturation and clogging in the microsystem. Hence the construction of the parametric dependencies of the global quantities, e.g., the maximum of the reaction rate between the calcium and the carbonate ions, has been carried out.

The dependence of the position of the maximum reaction rate of the reaction between the calcium and the carbonate ions on the total concentration of the carbonate in the R compartment is depicted in Fig. 2A. The solid line corresponds to the case without the imposed electric field. If $c_{CO_3,R} \in \langle 10^{-5}, 10^{-2} \rangle$ kmol m^{-3}, the position of the maximum rate of $CaCO_3$ formation is located in the middle of the microcapillary. The steady state spatial profiles of concentrations are almost linear because of the dominance of the diffusion transport. When the total concentration of carbonate increases, the global behavior of the microcapillary system becomes strongly dependent on the total carbonate concentration. The spatial distribution of carbonate is still linear while the calcium ions are quickly consumed by the

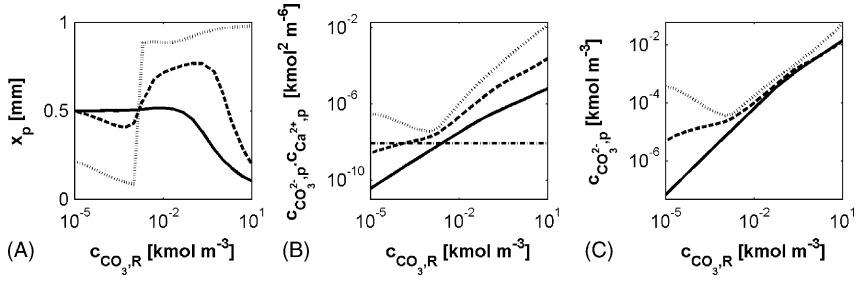

Fig. 2. Dependence of the steady state characteristics on the total concentration of carbonate in the R reservoir: (A) position of the maximum rate of the reaction between the calcium and the carbonate ions; (B) concentration product of the carbonate and calcium ions at the position of the maximum reaction rate; (C) concentration of carbonate ions at the position of the maximum reaction rate. The parameter values are l = 1 mm, $\Delta\Phi = 0$ V (solid line), $\Delta\Phi = 0.1$ V (dashed line), $\Delta\Phi = 1$ V (dotted line). The dash-dotted line in (B) depicts the solubility product of CaCO3. The subscript 'p' denotes a concentration at the position of the maximum reaction rate.

precipitation and higher Ca^{2+} concentration is observed only near the L reservoir. It results in the shift of the peak of $CaCO_3$ formation to the L reservoir.

As we can see in Fig. 2A, the dependence of the position of the maximum rate of $CaCO_3$ formation is more complex when the potential difference of an external electric field potential is applied. Let us focus on the case $\Delta\Phi = 1$ V (the dotted line). We can recognize a steep shift in the position of the peak of the $CaCO_3$ formation rate at the carbonate concentration value $c_{CO_3,R} \approx 10^{-3}$ kmol m^{-3}. This sharp change is caused by the switch of the electrolyte dominance, which can be explained by means of Fig. 3, where the steady state profiles of pH value, concentrations (normalized by characteristic boundary concentrations) and electric potential are shown.

If the $CaCl_2$ electrolyte in the L reservoir is dominant (e.g. $c_{CO_3,R} = 10^{-4}$ kmol m^{-3}), i.e., its concentration is higher than the concentration of the K_2CO_3 solution in the R reservoir, we can observe a number of interesting phenomena (the solid line in Fig. 3A–F). The chloride ions are concentrated by the electric force near the L compartment (Fig. 3C) whereas the calcium ions are pulled to the R compartment. The positive charge of calcium ions at higher distance from the L reservoir has to be compensated by the negative electric charge of the carbonate and the bicarbonate ions. Hence, their concentration inside the microreactor is much higher than in the R reservoir (Fig. 3F). The position of the peak on the rate profile of the $CaCO_3$ formation coincides with the concentration profile of the carbonate and the bicarbonate ions—the peak is observed near the L reservoir. Further, a high concentration of the carbonate and the bicarbonate ions accelerates their association reactions with the hydrogen ions, which results in an increase of the mean pH value in the microcapillary system (Fig. 3A). Because of the lower concentration of ions and the lower electric conductivity close to the R compartment, a locally higher potential of the electric field is found in this region in order to preserve the constant flow of the nonreacting ions in the steady state. A concave shape of the electric potential profile is then observed (Fig. 3D). Let us note that the above-described behavior of the microsystem follows from the electro-migration flow of the ionic components and cannot be observed in the systems without the imposed gradient of the electric potential.

Entirely opposite effects are identified when K_2CO_3 in the R reservoir is the dominant electrolyte (e.g., $c_{CO_3,R} = 10^{-1}$ kmol m^{-3}), see the dash-dotted line in Fig. 3A–F. The positively charged potassium ions are kept in the R reservoir (Fig. 3B) and the concentration of calcium ions in the microcapillary is much higher than the corresponding concentration in the reservoir (Fig. 3E). The carbonate ions are quickly consumed due to the formation of $CaCO_3$, then carbonic acid and the bicarbonate ions dissociate and the mean pH value decreases (Fig. 3A). A convex spatial profile of electric potential is reached due to low electric conductivity close to the L reservoir (Fig. 3D).

When the total concentration of electrolytes in both reservoirs is approximately the same (e.g., $c_{CO_3,R} = 10^{-3}$ kmol m^{-3}), one can observe a linear spatial profile of electric potential and the pH value almost constant along the entire profile (the dashed and the dotted curves of pH and electric potential in Fig. 3A and D). The increase of the concentrations of ions above their boundary concentrations is negligible.

The application of an external electric field has important effects on the global behavior of the system. The microreactor clogging can occur if the concentration product of calcium and carbonate ions locally exceeds the value of the solubility product K_s. The dependence of the maximum of the concen-

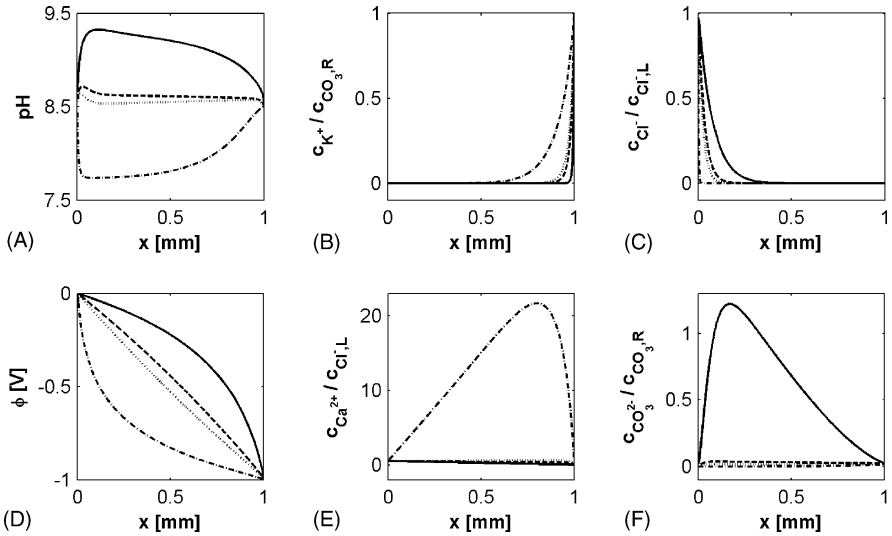

Fig. 3. Steady state distributions of the model variables for various total concentrations of carbonate in the R reservoir: (A) pH value; (B) the normalized concentration of potassium ions; (C) the normalized concentration of chloride ions; (D) electric potential; (E) the normalized concentration of calcium ions; (F) the normalized concentration of carbonate ions. Solid line $c_{CO_3,R} = 1 \times 10^{-4}$ kmol m^{-3}, dashed line $c_{CO_3,R} = 1 \times 10^{-3}$ kmol m^{-3}, dotted line $c_{CO_3,R} = 2 \times 10^{-3}$ kmol m^{-3}, dash-dotted line $c_{CO_3,R} = 1 \times 10^{-1}$ kmol m^{-3}. The parameter values are $l = 1$ mm, $\Delta\Phi = 1$ V.

tration product in the spatial profile on the total concentration of carbonate is plotted in Fig. 2B. As expected in the case of zero difference of the electric potential, the solubility product is not exceeded when the total carbonate concentration drops below a critical value (for our set of model parameters $c_{CO_3,R} < 5 \times 10^{-3}$ kmol m^{-3}). If an electric field is imposed on the microcapillary ($\Delta\Phi = 1$ V), the concentration product of the precipitating ions never decreases below the value of the solubility product in the studied interval of the total carbonate concentration. It means that the precipitation in the reaction microsystems with the imposed electric field can begin even if the concentration product of the calcium and carbonate ions in the reservoirs ($c_{Ca^{2+},L} \cdot c_{CO_3^{2-},R}$) is much lower than the solubility product and then the clogging of the microsystem can occur. The existence of the described phenomenon can be explained by means of Fig. 2C, where the concentration of carbonate ions at the position of maximum rate of formation of $CaCO_3$ is plotted. At given electric field strength and orientation, the concentration dominance of the electrolyte in one reservoir results in an increase in the concentration of the precipitating counterion from the other reservoir above its boundary concentration in order to balance the electric charge in the capillary microreactor.

4.2. Dynamical analysis

The main aim of the dynamical analysis is to determine at what time and position in the microstructure the precipitation of $CaCO_3$ can start.

The effects of both the total concentration of the carbonate in the R reservoir and the imposed potential gradient on the critical time t_p, at which the solubility product is reached, are depicted in Fig. 4A. The imposed potential gradient of given polarity accelerates the $CaCO_3$ formation. We can observe that t_p does not exceed 50 s on the studied interval of the total carbonate concentration for $\Delta\Phi = 1$ V. When $\Delta\Phi = 0$ V, t_p grows to infinity with the decreasing carbonate concentration. The growing total concentration of the carbonate thus accelerates the attainment of the solubility product, which follows from the combined effect of higher intensity of both the diffusion and the electro-migration transport (see Eq. (2)).

The spatial position of the maximum rate of $CaCO_3$ formation x_p depends on both the total carbonate concentration and the imposed difference of the electric potential. A single peak and low sensitivity with respect to the total carbonate concentration are observed in the systems with $\Delta\Phi = 0$ or 0.1 V.

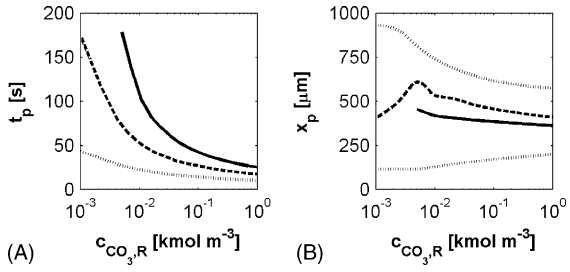

Fig. 4. Dependence of the dynamical characteristics on the total concentration of carbonate in the R reservoir: (A) time when the value of the solubility product is reached (critical time t_p); (B) Position of the reached solubility product in the capillary (x_p). The parameter values are l = 1 mm, $\Delta\Phi = 0$ V (solid line), $\Delta\Phi = 0.1$ V (dashed line), $\Delta\Phi = 1$ V (dotted line).

The example of dynamical evolution of spatial profiles of the selected model variables for $\Delta\Phi = 0$ V is plotted in Fig. 5A–D. Even if the diffusion mechanism of transport dominates, the electro-migration is also present especially at the start. This effect results from different mobilities of ions in the electrolytes and strongly nonlinear distribution of the mobile electric charge in the microreactor (see Eq. (4)). As the components of the both reservoir solutions are diffusing and migrating in the microcapillary, the distribution of electric potential is becoming a constant function of the spatial variable. The electro-migration transport is vanishing with the increasing time. The solubility product is reached at $t = 105$ s for the given set of model parameters. The concentration profiles of the calcium, carbonate, and the other ions remain monotonous in the studied time interval. When the solubility product is attained, no sharp gradients of ion concentrations arise. Let us note that the position of the spatial maximum of the rate of $CaCO_3$ formation at the time t_p is substantially different from its steady state position (compare Figs. 2A and 4B). From the experimental point of view, Fig. 4B is much more important because it shows that the formation of $CaCO_3$ should be observed first around the position of the earliest supersaturation.

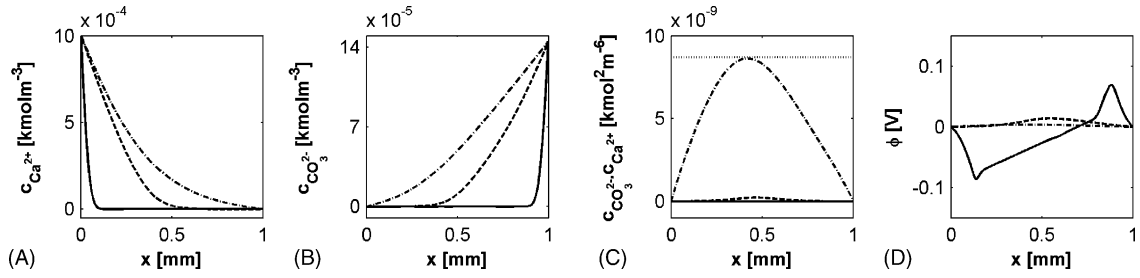

Fig. 5. Dynamical evolution of the distributions of the model variables in the microreactor: (A) concentration of calcium ions; (B) concentration of carbonate ions; (C) the concentration product of calcium and carbonate ions; (D) electric potential. Solid line $t = 0.5$ s, dashed line $t = 30$ s, dash-dotted line $t = 105$ s. The parameter values are l = 1 mm, $\Delta\Phi = 0$ V, $c_{CO_3,R} = 1 \times 10^{-2}$ kmol m^{-3}.

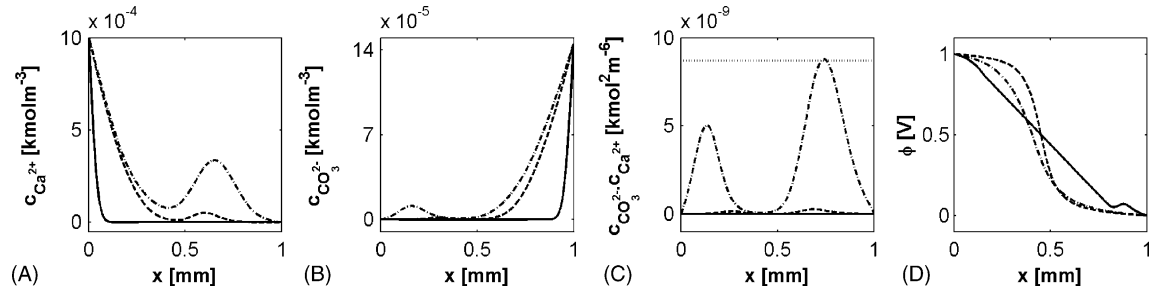

Fig. 6. Dynamical evolution of the distributions of the model variables in the microreactor: (A) concentration of calcium ions; (B) concentration of carbonate ions; (C) the concentration product of calcium and carbonate ions; (D) electric potential. Solid line $t = 0.5$ s, dashed line $t = 13.1$ s, dash-dotted line $t = 22.5$ s. The parameter values are $l = 1$ mm, $\Delta\Phi = 1$ V, $c_{CO_3,R} = 1 \times 10^{-2}$ kmol m^{-3}.

Two maxima on the spatial profile of the product of calcium and carbonate ion concentrations are observed, if $\Delta\Phi = 1$ V (see two dotted lines in Fig. 4B and the concentration profiles in Fig. 6A–C). Two peak pattern formation can be explained on the example in Fig. 6A–D. At the start of the system evolution, the precipitating ions are intensively transported from the reservoirs to the microcapillary due to higher electrostatic force. Thus the region close to the reservoirs is characterized by high electric conductivity. The local gradient of electric potential is low in these regions and the potential profile is assuming a sigmoidal shape (see Fig. 6D). The electrostatic force is much higher in the central part of the microcapillary than in the peripheral regions. Due to the mentioned distribution of the electrostatic force, the calcium and carbonate ions are intensely pulled through the central part of the microstructure with low electric conductivity. Hence the precipitating ions accumulate in the opposite peripheral parts of the microreactor (e.g., the calcium ions from the L compartment close to the R reservoir) where they balance the local electric charge, see Fig. 6A and B. The observed accumulation of these ions results in the two peak pattern formation.

The dependencies of the critical time t_p on principal model parameters have also been studied. If we consider a linear distribution of the electric potential, the combined diffusion–electro-migration transport time of the chemical component (e.g., of the hydrogen ions) can be then expressed as

$$t = \left(\frac{D_{H^+}}{l^2} + \frac{F D_{H^+} |\Delta\Phi|}{RTl^2} \right)^{-1}. \quad (20)$$

As the electric potential difference growths, the electro-migration term becomes dominant and the transport time should be proportional to the $\Delta\Phi$ according to relationship $t \approx \Delta\Phi^{-1}$. The computed dependence of the critical time on the imposed potential difference is plotted in Fig. 7A. The logarithmic plot confirms that the critical time does not depend on the imposed potential difference for $\Delta\Phi < 10^{-2}$ V when the molecular diffusion is dominant. If $\Delta\Phi \in \langle 0.02, 20 \rangle$ V, the critical time is then proportional to the imposed potential gradient according to $t \approx \Delta\Phi^{-1/3}$. The slope of the described dependence is steeper for $\Delta\Phi > 20$ V. Hence Eq. (20) cannot be used for the estimation of the critical and/or transport time.

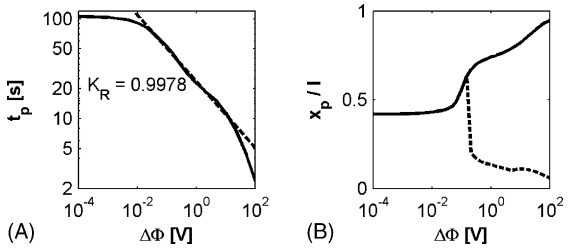

Fig. 7. Dynamical analysis, effects of the imposed difference of electric potential: (A) dependence of the critical time t_p on the imposed difference of electric potential ($c_{CO_3,R} = 1 \times 10^{-1}$ kmol m^{-3}, $l = 1$ mm); (B) dependence of the relative position of reaction maxima x_p/l of the calcium–carbonate interaction on the imposed difference of electric potential at the critical time t_p ($c_{CO_3,R} = 1 \times 10^{-1}$ kmol m^{-3}, $l = 1$ mm). The solid line—the main peak, the dashed line—the lower peak.

The solubility product is attained at the critical time. The computed dependence of the relative position of the reaction rate peak of the calcium–carbonate interaction x_p/l on the imposed difference of electric potential is depicted in Fig. 7B. The peak splitting takes place when $\Delta\Phi > 10^{-1}$ V. This bifurcation point lies in the region of dominance of the electro-migration transport (see Fig. 7A). As discussed earlier, the reaction peak splitting follows from the formation of the steep gradient of electric potential within the microcapillary (strongly sigmoidal profile of electric potential). When the imposed difference of electric potential growths, a smaller peak is disengaged and the spatial distance between this new peak and the original one swiftly increases (see the courses of the solid and the dashed lines in Fig. 7B).

The effects of another model parameter, the length of the microcapillary l, are shown in Fig. 8. Although the two peak pattern was observed, we have plotted here only the global maximum of the rate of $CaCO_3$ formation in the microreactor. The dependence of the critical time t_p on the length of the microcapillary in the logarithmic scale is plotted in Fig. 8A. This dependence is approximately linear and its slope is about 2 on the studied interval of the microcapillary length and Eq. (20) holds.

We have found that the increasing length of the microcapillary does not affect the observed number of peaks on the

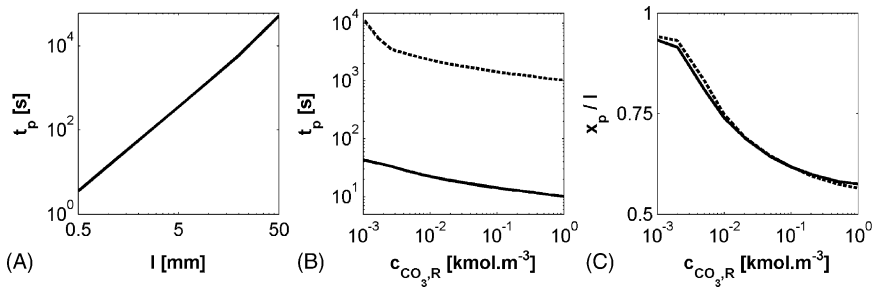

Fig. 8. Dynamical analysis, effects of the microcapillary length: (A) dependence of the critical time t_p on the length of the microcapillary ($c_{CO_3,R} = 1 \times 10^{-1}$ kmol m^{-3}, $\Delta\Phi = 1$ V); (B) dependence of the critical time t_p on the total concentration of carbonate in the R reservoir, solid line (l = 1 mm, $\Delta\Phi = 1$ V), dashed line (l = 10 mm, $\Delta\Phi = 1$ V); (C) dependence of the relative position of the solubility limit in the reaction microsystem x_p/l on the total concentration of carbonate in the R reservoir, solid line (l = 1 mm, $\Delta\Phi = 1$ V), dashed line (l = 10 mm, $\Delta\Phi = 1$ V).

profile of the product of the calcium and the carbonate ions. It corresponds with the existence of only single decrease of the electric potential on its sigmoidal spatial profile in the case of $\Delta\Phi = 1$ V.

The dependences of the critical time t_p on the total carbonate concentration in the R reservoir for two microreactor lengths are depicted in Fig. 8B. The course of these dependences has a similar shape for both microreactors. As expected, the critical time is higher by several orders of magnitude for the longer capillary. The microsystem with the given set of parameters is sensitive with respect to the concentration of electrolyte in both reservoirs. The relative position of the peak on the reaction rate profile x_p/l almost does not depend on the microcapillary length (see Fig. 8C). Small differences result from the used boundary conditions at the ends of the microcapillary.

5. Conclusions

In the steady states analysis of the studied microcapillary system, we have found that the position of the maximum reaction rate of the interaction between the calcium and the carbonate ions strongly depends on the electrolyte dominance (the dominant electrolyte is characterized by a higher concentration than the other one). This effect is increased under an applied electric field of a specific orientation. Some components of the electrolyte with a lower concentration are forced by the electrostatic force to increase their concentration over their boundary (reservoir) concentrations. This increase can cause that the solubility limit is exceeded. It means that the precipitation in the reaction microsystems with an imposed electric field can occur for much lower concentration of the electrolytes in the reservoirs than in the system without an imposed electric field. Hence the possibility of the microreactor clogging increases. An imposed electric field can also induce large changes of the pH value inside the microstructure. These changes can finally result in the precipitation of calcium carbonate in the system. The experimental observation of the precipitation caused by the electrokinetic phenomena and pH shift were recently reported by Cherepy and Wildenschild [39]. They studied an electroosmotic flow in a clay bed containing micropores. The authors found that the electrokinetic phenomena can induce carbonate precipitation at a specific position in the clay bed.

The dependences of the critical time, at which the solubility product of $CaCO_3$ is exceeded, and the position of the first appearance of the saturation in the microcapillary on several model parameters are studied in the dynamical analysis. In this work, we assume that the risk of clogging is likely at any point where the solubility product is exceeded. We have observed two different spatio-temporal patterns in the microreactor in dependence on the applied difference of the electric potential. A single peak on the reaction rate profile was detected for low potential differences $\Delta\Phi/l \leq 0.1$ V/1 mm. A two peak pattern was observed for higher values of $\Delta\Phi/l$. This follows from the existence of the sigmoidal profile of the electric potential in the microstructure. Due to the sigmoidal distribution of the electrostatic force, the calcium and carbonate ions are intensely pulled through the central part of the microcapillary characterized by low electric conductivity and the precipitating ions accumulate in the opposite peripheral parts, which leads to the two peak pattern formation.

The development of the two peak spatio-temporal pattern is not based on the same principle as in the case of Liesegang patterns. The description of periodic Liesegang patterns is based on the reaction–diffusion principles in a supersaturated solution. The precipitate formation starts at the position of the local supersaturation and the free reactants from the vicinity of this zone are consumed, which results in the alternation of the zones with and without the solid precipitate. In our case, the splitting of the zone with possible precipitation is caused by the existence of the sigmoidal distribution of the electric potential. We expect that the formation of spatial patterns with even higher degree of complexity is possible in the microcapillary. These patterns can result both from the sigmoidal profile of the electric potential and the Oswald's principles. Then the final pattern can be formed within two separate regions containing the Liesegang periodic structures. As we did not describe the processes in the supersaturated solution, we cannot definitely conclude that the precipitation in the two separate regions will occur.

We have found that the dependence of the critical time, when the solubility product is attained, on the imposed difference of electric potential in the region of dominant electromigration transport can be expresses by a simple relationship $t \approx \Delta\Phi^{-1/3}$. It means that the decrease of the critical time for the sigmoidal profile is much slower than for the linear profile.

Our findings can be useful for scientists who are interested in the processes in the microcapillaries containing aqueous electrolytes with a high ratio of the axial/radial dimensions (capillary electrophoresis, isoelectrical focusing, diagnostic chips, nanoparticles production, etc.). The avoidance of the microchip clogging in the blood plasma analysis is one of the possible applications of the presented results. Possible control of the processes leading to precipitation in microdevices (e.g. [14–19]) by the imposed electric field can help to avoid the unwanted clogging. We plan to include the description of supersaturation processes in a future model and to test the above predictions by experiments.

Acknowledgement

Two of the authors (M. Přibyl and M. Marek) thank to the Ministry of Education, Youth, and Sport of the Czech Republic (grant no. 1K03003) for support of this project. D. Šnita thanks to the Czech Science Foundation for support of his research (grant no. 104/04/1442).

References

[1] M. Sinder, Phys. Rev. E 65 (2002) 037104-1-037104-4.
[2] M. Sinder, J. Pelleg, Phys. Rev. E 68 (2003) 022101-1-022101-4.
[3] M. Sinder, J. Pelleg, Phys. Rev. E 62 (2000) 3340–3348.
[4] H. Taitelbaum, B. Vilensky, A. Lin, A. Yen, Y.L. Koo, R. Kopelman, Phys. Rev. Lett. 77 (1996) 1640–1643.
[5] A. Yen, A.L. Lin, Y.L. Koo, B. Vilensky, H. Taitelbaum, R. Kopelman, J. Phys. Chem. A 101 (1997) 2819–2827.
[6] M.J. Heller, A. Guttman, Integrated Microfabricated Biodevices, Marcel Dekker, New York, 2002.
[7] J. Rossier, F. Reymond, P.E. Michel, Electrophoresis 23 (2002) 858–867.
[8] P.D.I. Fletcher, S.J. Haswell, X. Zhang, Lab on Chip 2 (2002) 102–112.
[9] R.M. Guijt, E. Baltussen, G.W.K. van Dedem, Electrophoresis 23 (2002) 823–835.
[10] M. Přibyl, D. Šnita, P. Hasal, M. Marek, Chem. Eng. J. 101 (2004) 303–314.
[11] W.F. Ganong, Review of Medical Physiology, 7th ed., Lange Medical Publications, Los Altos, CA, 1975.
[12] J.F. VanGulck, R.K. Rowe, B.E. Rittmann, A.J. Cooke, Biodegradation 14 (2003) 331–346.
[13] X. Lin, R.C. Burns, G.A. Lawrance, Water Res. 32 (1998) 3637–3645.
[14] E.M. Chan, R.A. Mathies, A.P. Alivisatos, NanoLetters 3 (2003) 199–201.
[15] M. Takagi, T. Maki, M. Miyahara, K. Mae, Chem. Eng. J. 101 (2004) 269–276.
[16] J. Wagner, T. Kirner, G. Mayer, J. Albert, J.M. Köhler, Chem. Eng. J. 101 (2004) 251–260.
[17] R. Schenk, V. Hessel, Ch. Hofmann, J. Kiss, H. Löwe, A. Ziogas, Chem. Eng. J. 101 (2004) 421–429.
[18] S. Guillemet-Fritsch, M. Aoun-Habbache, J. Sarrias, A. Rousset, N. Jongen, M. Donnet, P. Bowen, J. Lemaitre, Solid State Ionics 171 (2004) 135–140.
[19] R. Schenk, M. Donnet, V. Hessel, Ch. Hofmann, N. Jongen, H. Löwe, in: M. Matlosz, W. Ehrfeld, J. Baselt (Eds.), Microreaction Technology: IMRET 5, Springer, Berlin, 2002, pp. 489–498.
[20] P. Magnico, Chem. Eng. Sci. 55 (2000) 4323–4338.
[21] J.H.D. Hampton, S.B. Savage, Chem. Eng. Sci. 48 (1993) 1601–1611.
[22] K. Stole-Hansen, Comput. Chem. Eng. 20 (1996) S629–S634.
[23] J.W. Yu, I. Neretnieks, Chem. Eng. Sci. 51 (1996) 4355–4368.
[24] R.E. Liesegang, Naturwiss. Wochenschr. 11 (1896) 353.
[25] S.C. Műller, J. Ross, J. Phys. Chem. A 107 (2003) 7997–8008.
[26] R. Sultan, R. Halabieh, Chem. Phys. Lett. 332 (2000) 331–338.
[27] I. Lagzi, Phys. Chem. Chem. Phys. 4 (2002) 1268–1270.
[28] M. Al-Ghoul, R. Sultan, J. Phys. Chem. A 107 (2003) 1095–1101.
[29] I. Lagzi, F. Izsák, Phys. Chem. Chem. Phys. 5 (2003) 4144–4148.
[30] J. Kosek, H. Ševčiková, M. Marek, J. Phys. Chem. 99 (1995) 6889–6896.
[31] P. Ortoleva, R. Sultan, Chem. Phys. 148 (1990) 47–55.
[32] J. Lindner, D. Šnita, M. Marek, Phys. Chem. Chem. Phys. 4 (2002) 1348–1354.
[33] D. Šnita, M. Pačes, J. Lindner, J. Kosek, M. Marek, Faraday Discuss. 120 (2002) 53–66.
[34] W.M. Deen, Analysis of Transport Phenomena, Oxford University Press, New York, 1998.
[35] G.H. Nancollas, M.M. Reddy, J. Colloid Interf. Sci. 37 (1971) 824–830.
[36] T.H. Chong, R. Sheikholeslami, Chem. Eng. Sci. 56 (2001) 5391–5400.
[37] P.N. Brown, A.C. Hindmarsh, L.R. Petzold, SIAM J. Sci. Comput. 15 (1994) 1467–1488.
[38] A. Dodge, K. Fluri, E. Verpoorte, N.F. de Rooij, Anal. Chem. 73 (2001) 3400–3409.
[39] N.J. Cherepy, D. Wildenschild, Environ. Sci. Technol. 37 (2003) 3024–3030.